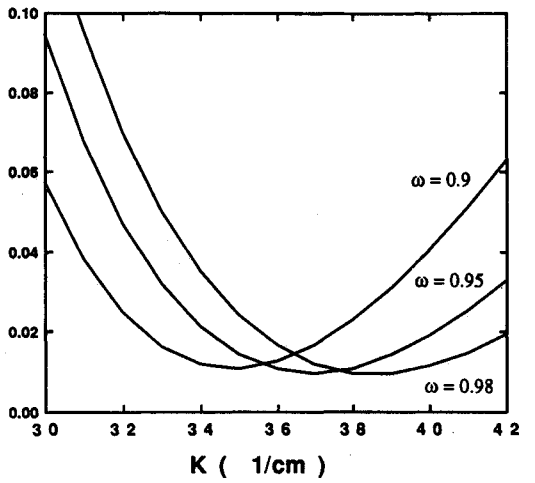

Fig. 3 Error sum calculated for different K and ω.

width of the scattering sample (KL) was not recorded in the experiment, therefore numerical data for an one-dimensional slab ($KL \to \infty$) are used in the calculation.

An initial estimate for the extinction coefficient K is obtained by interpolating the LI900 transmission data in the optically thin limit. For each assumed K and ω, an error sum is calculated by

$$S = \sum_{\text{data}} (\tau_{\text{measure}} - \tau_{\text{numerical}})^2 \qquad (12)$$

with the summation extended to all measured data points. The behavior of S for different ω and K is shown in Fig. 3. It is apparent that the present approach is numerically stable. It yields a unique least-square prediction for $\omega = 0.95$ and $K = 37\ \text{cm}^{-1}$. A Mie calculation, based on the known fiber size distribution of the test sample, yields $\omega = 1.0$, $K = 148\ \text{cm}^{-1}$, and $b = 0.173$. The discrepancy in K can probably be attributed to the anisotropic scattering effect which is not included in the model and the uncertainty of the index of refraction utilized in the Mie calculation. Nevertheless, the agreement in ω and the ability of the model to predict the qualitative behavior of the transmissivity suggest that the current mathematical model and experimental approach is a promising procedure for the determination of optical properties. It is also apparent that this procedure can be readily extended to applications for anisotropically scattering materials.

IV. Conclusions and Future Works

A unique experimental and numerical procedure is shown to be effective in predicting optical properties for a two-dimensional absorbing and isotropically scattering medium. Analysis of some limited data generated for a fibrous insulation material (LI900) shows the potential of present approach.

Additional experiments are needed to verify the statistical reliability and sensitivity of the proposed experimental technique. Since most insulation materials scatter anisotropically, an extension of the numerical procedure to general absorbing, anisotropically scattering media is required. The recently developed generalized zonal method[8] appears to be ideally suited for the extension. These efforts are currently underway and results will be reported in future publications.

References

[1]Tong, T. W., and Tien, C. L., "Radiative Heat Transfer in Fibrous Insulations. Part I: Analytical Study," *ASME Journal of Heat Transfer*, Vol. 105, 1983, pp. 70–75.

[2]Cunnington, G. R., Tong, T. W., and Swathi, P. S., "Angular Scattering of Radiation from Cylindrical Fibers," AIAA Paper 88-2721, 1988.

[3]Yuen, W. W., "Development of a Network Analogy and Evaluation of Mean Beam Length for Multi-Dimensional Absorbing/Isotropically Scattering Media," *ASME Journal of Heat Transfer*, Vol. 112, May 1990, pp. 408–414.

[4]Hottel, H. C., and Sarofim, A. F., *Radiative Transfer*, McGraw-Hill, New York, 1967.

[5]Yuen, W. W., and Wong, L. W., "Numerical Computation of an Important Integral Function in Two-Dimensional Radiative Transfer," *Journal of Quantitative Spectroscopy and Radiative Transfer*, Vol. 29, No. 2, 1983, pp. 145–149.

[6]Yuen, W. W., Ma, A., Hsu, I. C., and Cunnington, G. R., "Evaluation of Optical Properties for Scattering/Absorbing Insulation Materials with Two-Dimensional Scattering," AIAA Paper 90-1719, June 18–20, 1990.

[7]Lockheed, private communication.

[8]Yuen, W. W., and Takara, E. E., "Development of a Generalized Zonal Method for the Analysis of Radiative Transfer in Absorbing and Anisotropically Scattering Media," the 1990 ASME/AIAA Thermophysics and Heat Transfer Conference, Seattle, WA, June 18–20, 1990.

Transient Laminar Forced Convection From a Circular Cylinder Using a Body-Fitted Coordinate System

Yue-Tzu Yang,* Cha'o-Kuang Chen,† and Sang-Ru Wu‡
National Cheng-Kung University, Tainan, Taiwan, Republic of China

Introduction

THE problem of steady flow and heat transfer characteristics around a circular cylinder has been widely investigated. At the situation of Reynolds number $5 < Re < 40$ there exists a pair of steady and symmetric vortices right behind the cylinder. When $Re > 40$, the flow begins to have an unsteady motion. The vortices are oscillating periodically and flowing in the downstream direction. Thoman and Szewczyk,[1] Gresho et al.,[2] and Hwang et al.[3] studied the time-dependent flow characteristics of a circular cylinder. Jordan and Fromm,[4] Lin et al.,[5] Patel,[6] Lecointe and Piquet,[7] and Smith and Brebbia[8] have presented their numerical results for the unsteady incompressible viscous flow past a circular cylinder.

Jain and Goel,[9] McAdam,[10] Kramers,[11] Van der Hegge Zijnen,[12] and Tsubouchi and Masuda[13] discussed the development of the vortex shedding behind a circular cylinder. Karniadakis[14] used the spectral element method to solve forced convection heat transfer from an isolated cylinder in crossflow for Reynolds numbers up to 200. In the present paper, the problem of transient laminar forced convection from a horizontal isothermal cylinder is studied. The Navier-Stokes equations and the energy equation for an unsteady incompressible fluid flow are solved by using a body-fitted orthogonal coordinate system and spline alternating direction implicit (SADI) method, described by Rubin and Graves.[15] The computed results are compared with previous experimental correlations and numerical results. Although there are many investigations concerning this subject, the main contribution of the present paper is that a different numerical technique is applied and the results are extended to $Re = 500$.

Received Aug. 30, 1990; revision received Jan. 4, 1991; accepted for publication Jan. 28, 1991.

*Associate Professor, Department of Mechanical Engineering.
†Professor, Department of Mechanical Engineering.
‡Graduate Student, Department of Mechanical Engineering.

Mathematical Formulation

Consider the problem of a cylinder of radius R and an isothermal surface with temperature T_s, placed in a uniform freestream of temperature T_∞ and velocity U. The cylinder is considered to be long enough so that the end effects can be neglected and the temperature difference is assumed to have a negligible effect on the fluid properties and the fluid is incompressible. Assuming that the buoyance force is small compared with the inertia force, that is $Gr/Re^2 << 1$, forced convection occur. The dimensionless governing equations can be written as follows:

Energy equation

$$\frac{\partial T}{\partial t} + \frac{\partial \psi}{\partial y}\frac{\partial T}{\partial x} - \frac{\partial \psi}{\partial x}\frac{\partial T}{\partial y} = \frac{2}{RePr}\left(\frac{\partial^2 T}{\partial x^2} + \frac{\partial^2 T}{\partial y^2}\right) \tag{1}$$

Vorticity equation

$$\frac{\partial \omega}{\partial t} + \frac{\partial \psi}{\partial y}\frac{\partial \omega}{\partial x} - \frac{\partial \psi}{\partial x}\frac{\partial \omega}{\partial y} = \frac{2}{Re}\left(\frac{\partial^2 \omega}{\partial x^2} + \frac{\partial^2 \omega}{\partial y^2}\right) \tag{2}$$

Stream function equation

$$\frac{\partial^2 \psi}{\partial x^2} + \frac{\partial^2 \psi}{\partial y^2} = -\omega \tag{3}$$

The equations are nondimensionalized in terms of the following dimensionless quantities:

$$x^* = \frac{x}{R},\quad y^* = \frac{y}{R},\quad r^* = \frac{r}{R},\quad u^* = \frac{u}{U},\quad v^* = \frac{v}{U},$$

$$p^* = \frac{p}{\rho U^2},\quad \omega^* = \frac{\omega R}{U},\quad \psi^* = \frac{\psi}{UR},\quad T^* = \frac{T - T_\infty}{T_s - T_\infty}$$

$$t^* = \frac{tU}{R} \tag{4}$$

In the following the notation * is omitted for convenience. The dimensionless initial conditions at $t < 0$ are:

$$\psi = 0,\quad \omega = 0,\quad T = 0 \tag{5}$$

The boundary conditions on the cylinder are on the boundary Γ_1 at $t \geq 0$

$$T = 1,\quad \psi = 0,\quad \omega = -\nabla^2 \psi \tag{6}$$

on the boundary Γ_3, Γ_4, Γ_6, and Γ_7 at $t \geq 0$

$$T = 0,\quad \psi = \left(r - \frac{1}{r}\right)\sin\theta$$
$$\omega = 0 \tag{7}$$

on the boundary Γ_5 at $t \geq 0$

$$\frac{\partial T}{\partial x} = 0,\quad \frac{\partial \psi}{\partial x} = 0,\quad \frac{\partial \omega}{\partial x} = 0 \tag{8}$$

Numerical Procedure

The governing equations, and initial and boundary conditions can be expressed in terms of a body-fitted coordinate developed by Thompson et al.[16] as shown in Fig. 1. The domain of solution considered in this study extended to a downstream distance of approximately 38 R from the center of cylinder and to a upstream distance of 10 R. Fig. 1a shows that multiply connected regions can be treated by segmentation into simply connected subregions for which the Di richlet problem remains well posed. In order to create grid lines conveniently, the whole computational domain was divided into two subregions, region 1 and region 2. Region 1 is a simply connected region and region 2 is a multiply connected region around the cylinder. Curve GD is the interface of the two subregions. It was assumed to satisfy the elliptical curve

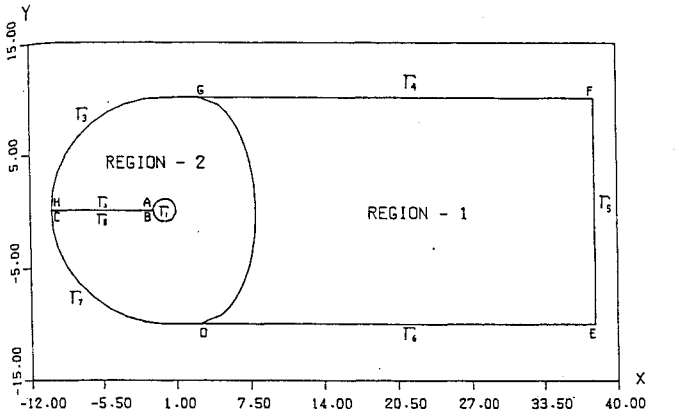

a) Physical plane

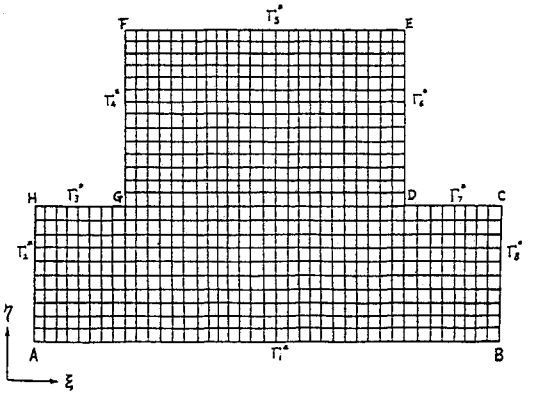

b) Transformed plane

Fig. 1 Transformation of the solution domain.

$$\frac{(x - b)^2}{a^2} + \frac{y^2}{10^2} = 1 \tag{9}$$

where $a = 5$, $b = 3$.

The boundary-fitted physical coordinate system is created by solving the following system of Poisson equations:

$$\xi_{xx} + \xi_{yy} = P(\xi,\eta) \tag{10a}$$

$$\eta_{xx} + \eta_{yy} = Q(\xi,\eta) \tag{10b}$$

where P and Q are the coordinate control functions that provide the control of the mesh concentrations. Since it is desired to perform all numerical calculations in the transformed plane, the dependent and independent variables must be interchanged in Eqs. (10a) and (10b). The transformed equations are

$$\alpha x_{\xi\xi} - 2\beta x_{\xi\eta} + \gamma x_{\eta\eta} = -J^2(Px_\xi + Qx_\eta) \tag{11a}$$

$$\alpha y_{\xi\xi} - 2\beta y_{\xi\eta} + \gamma y_{\eta\eta} = -J^2(Py_\xi + Qy_\eta) \tag{11b}$$

where

$$\alpha = x_\eta^2 + y_\eta^2;\quad \beta = x_\xi x_\eta + y_\xi y_\eta;\quad \gamma = x_\xi^2 + y_\xi^2;$$
$$J = \partial(x,y)/\partial(\xi,\eta) = x_\xi x_\eta - x_\eta x_\xi \neq 0$$

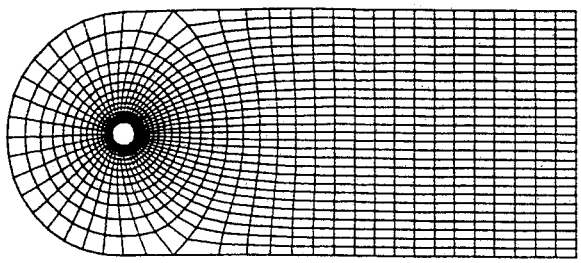

Fig. 2 The body-fitted coordinate system.

The difficulty of interior grid control has been overcome by devising general source terms P and Q that are computed from the Dirichlet boundary values. The source terms have the form

$$P = \bar{\phi}(\xi,\eta)\,(\xi_x^2 + \xi_y^2)$$
$$Q = \bar{\psi}(\xi,\eta)\,(\eta_x^2 + \eta_y^2) \tag{12}$$

where the parameters $\bar{\phi}$ and $\bar{\psi}$ are yet to be specified. Based on introducing these terms, Eqs. (11a) and (11b) assume the form

$$\alpha(x_{\xi\xi} + \bar{\phi}x_\xi) - 2\beta x_{\xi\eta} + \gamma(x_{\eta\eta} + \bar{\psi}x_\eta) = 0$$
$$\alpha(y_{\xi\xi} + \bar{\phi}y_\xi) - 2\beta y_{\xi\eta} + \gamma(y_{\eta\eta} + \bar{\psi}y_\eta) = 0 \tag{13}$$

It is clearly shown that Eq. (13) possesses expotential solutions if the parameter $\bar{\phi}$ and $\bar{\psi}$ are locally constant. If a set of boundary values (x,y) on the boundary of the computational domain is given, one can determine the parameters by requiring that the given boundary values satisfy appropriate limiting forms of Eq. (13) along the boundary of the computational domain.

The transformed equations [Eqs. (10a) and (10b)] were solved with the Successive Over Relaxation (SOR) method. Once a grid is generated, the values of the coefficients α, β, γ, and J, etc. are evaluated and stored for use in the solution of the governing equations.

The governing equations [Eqs. (1–3)] in terms of the transformed coordinates are

$$T_t + \frac{1}{J}(\psi_\eta T_\xi - \psi_\xi T_\eta) = \frac{2}{RePr}\left[\frac{1}{J^2}(\alpha T_{\xi\xi} + \gamma T_{\eta\eta}) + P(\xi,\eta)T_\xi + Q(\xi,\eta)T_\eta\right] \tag{14}$$

$$\omega_t + \frac{1}{J}(\psi_\eta \omega_\xi - \psi_\xi \omega_\eta) = \frac{2}{Re}\left[\frac{1}{J^2}(\alpha\omega_{\xi\xi}) + \gamma\omega_{\eta\eta} + P(\xi,\eta)\omega_\xi + Q(\xi,\eta)\omega_\eta\right] \tag{15}$$

$$\frac{1}{J^2}(\alpha\psi_{\xi\xi} + \gamma\psi_{\eta\eta}) + P(\xi,\eta)\psi_\xi + Q(\xi,\eta)\psi_\eta = -\omega \tag{16}$$

where

$$\alpha = x_\eta^2 + y_\eta^2, \quad \gamma = x_\xi^2 + y_\xi^2$$
$$P(\xi,\eta) = \bar{\phi}(\xi,\eta)\frac{\alpha}{J^2}, \quad Q(\xi,\eta) = \bar{\psi}(\xi,\eta)\frac{\gamma}{J^2}$$

In terms of the transformed coordinates, the initial conditions become at $t < 0$

$$\psi = 0, \quad \omega = 0, \quad T = 0 \tag{17}$$

and the boundary conditions become, on the boundary Γ_1^* at $t \geq 0$

$$T = 1, \quad \psi(\xi,1,t) = 0, \quad \psi_\eta = \psi_\xi = 0$$
$$\omega(\xi,1,t) = -\frac{1}{J^2}(\alpha\psi_{\xi\xi} + \gamma\psi_{\eta\eta}) \tag{18}$$

on the boundary Γ_3^*, Γ_4^*, Γ_6^*, and Γ_7^* at $t \geq 0$

$$T(\xi,\eta,t) = 0, \quad \omega(\xi,\eta,t) = 0$$
$$\psi(\xi,\eta,t) = \left(r - \frac{1}{r}\right)\sin\theta$$
$$\psi_\xi = uy_\xi - vx_\xi, \quad \psi_\eta = uy_\eta - vx_\eta \tag{19}$$

on the boundary Γ_5^*, at $t \geq 0$

$$T_\eta = 0, \quad \psi_\eta = 0, \quad \omega_\eta = 0 \tag{20}$$

The transformed governing equations, initial conditions, and boundary conditions were discretized by using the cubic spline collocation formulation. The SADI procedure was applied to perform the numerical computation. All computations reported here were performed with a mesh consisting of 51 × 33 grid lines as shown in Fig. 2 and a time increment $\Delta t = 0(1/2Re)$. Significantly finer grids could not be used because of computer storage and time limitation.

The convergence criterion for stream function, vorticity, and temperature is

$$\frac{\max_{i,j}|\psi_{i,j}^{s+1} - \psi_{i,j}^{s}|}{\max_{i,j}|\psi_{i,j}^{s+1}|} \leq 10^{-4} \tag{21}$$

$$\frac{\max_{i,j}|\omega_{i,j}^{k+1} - \omega_{i,j}^{k}|}{\max_{i,j}|\omega_{i,j}^{k+1}|} \leq 10^{-3} \tag{22}$$

$$\frac{\max_{i,j}|T_{i,j}^{k+1} - T_{i,j}^{k}|}{\max_{i,j}|T_{i,j}^{k+1}|} \leq 10^{-4} \tag{23}$$

where s and k are the number of iterations. After convergence of the numerical solution has been achieved, the following physical parameters were calculated.

Physical Parameters

1) Nusselt number

$$Nu = \frac{2Rh}{k} \tag{24}$$

2) Average Nusselt number

$$\overline{Nu} = \frac{1}{2\pi}\int_0^{2\pi} Nu\, d\theta \tag{25}$$

3) Drag coefficient

$$C_D = -\int_0^{2\pi} p\cos\theta\, d\theta - \frac{2}{Re}\int_0^{2\pi} \omega\sin\theta\, d\theta \tag{26}$$

4) Lift coefficient

$$C_L = -\int_0^{2\pi} p\sin\theta\, d\theta + \frac{2}{Re}\int_0^{2\pi} \omega\cos\theta\, d\theta \tag{27}$$

5) Torque coefficient

$$C_T = \frac{2}{Re}\int_0^{2\pi} \omega\, d\theta \tag{28}$$

6) Strouhal number

$$S = \frac{2Rf}{U} = \frac{2}{T'} \tag{29}$$

where f = vortex shedding frequency and T' = period of oscillation.

Results and Discussion

The problem of transient laminar forced convection from an isothermal circular cylinder is studied at Re = 100, 200, and 500 with Pr = 0.70. The present results for drag and lift coefficients and Strouhal number are compared with the previous results in Table 1. The comparisons are found to be satisfactory.

The time-dependent variation of velocity flow in the wake of a cylinder at Re = 500 is shown in Fig. 3. It is clear that unsymmetric vortex shedding happens early when the Reynolds number is increased.

Isotherm patterns are plotted in Fig. 4. By observing the isotherm pattern, an unsymmetrical flow in the wake gives rise to an unsymmetrical pattern. A significant distortion in the symmetry of the isotherms around the cylinder is observed as the process of the shedding of vortices takes place. It demonstrates that a significant change in the pattern of isotherms takes place in the region of the wake only.

The angular distribution of local Nusselt numbers for Re = 500 is shown in Fig. 5. The maximum and minimum values of the local Nusselt numbers along the surface of cylinder occur at the front stagnation point and the separation point.

The time-dependent average Nusselt numbers for Re = 100, 200, and 500 are shown in Fig. 6. It demonstrates that the greater Re is, the greater Nu. The average Nusselt numbers obtained in the present work are in good agreement with those obtained by the previous investigations as shown in Table 2.

Table 1 Comparisons of drag and lift coefficients C_D, C_L, and Strouhal number S

Re	C_D	C_L	S	Reference
100	1.28	±0.54	0.16	Jordan & Fromm[4]
	1.29	±0.50	0.133	Patel[6]
	1.43	±0.50	0.166	Smith & Brebbia[8]
	1.27	±0.6	0.161	Gresho et al.[2]
	1.30	±0.4	0.16	Hwang et al.[3]
	1.37	——	0.18	Karniadakis[14]
	1.282	±0.5	0.166	Present work
200	1.17	——	0.18	Lin et al.[5]
	1.27	±0.7	0.154	Patel[6]
	1.17	——	0.15	Thoman & Szewczyk[1]
	1.46	±0.7	0.194	Lecointe & Piquet[7]
	1.28	±0.6	0.182	Hwang et al.[3]
	1.17	——	0.20	Karniadakis[14]
	1.25	±0.67	0.185	Present work
500	1.25	±0.9	0.20	Hwang et al.[3]
	1.21	±0.88	0.21	Present work

Table 2 Comparisons of average Nusselt number

Reference	$\overline{Nu}$ (Re = 100)	$\overline{Nu}$ (Re = 200)	$\overline{Nu}$ (Re = 500)
McAdam[10]	5.23	7.2182	11.163
Kramers[11]	5.49	7.6025	11.794
Van der Hegge Zijnen[12]	5.45	7.6211	12.0303
Tsubouchi & Masuda[13]	5.16	7.1482	11.0931
Jain & Goel[9]	5.52	7.63	——
Karniadakis[14]	5.91	8.38	——
Present work	5.30	7.74	12.48

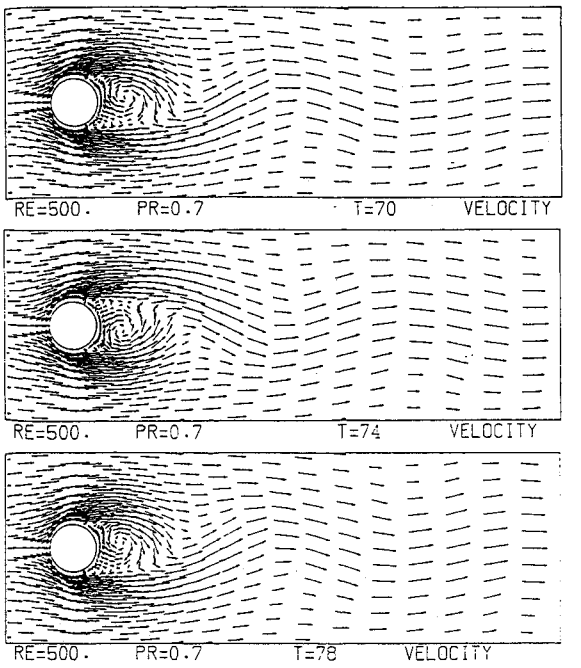

Fig. 3 The time-dependent variation of velocity field in the wake of a cylinder at Re = 500.

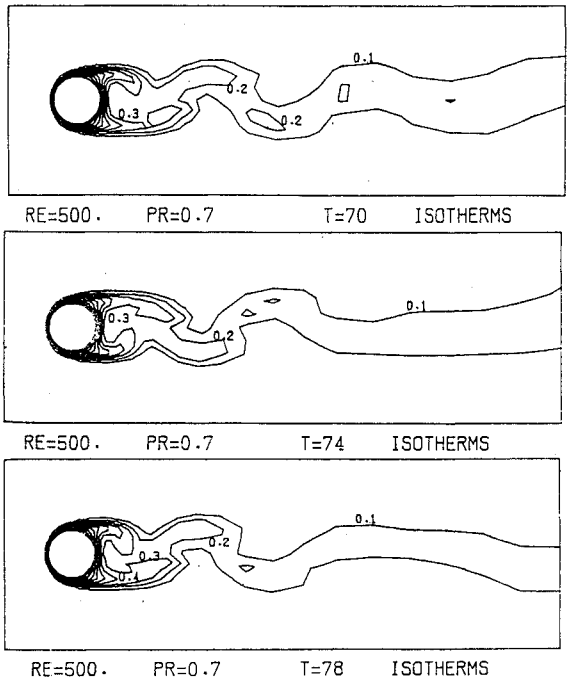

Fig. 4 The time-dependent isotherms at Re = 500.

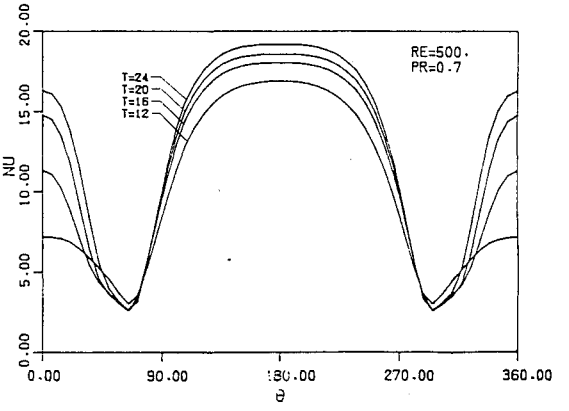

Fig. 5 Angular distribution of the local Nusselt number at Re = 500.

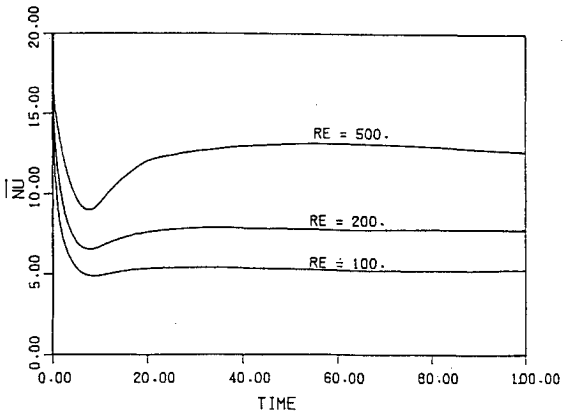

Fig. 6 The time-dependent average Nusselt numbers for Re = 100, 200, and 500.

Conclusion

A numerical solution has been obtained for the problem of transient laminar forced convection from a circular cylinder. The governing equations expressed in the body-fitted coordinates were solved numerically by the SADI method. The SADI method was applied to increase the accuracy, simplify the treatment of the boundary conditions, and save CPU time. The comparisons between the present results and previous investigation are found to be satisfactory.

References

[1]Thoman, D., and Szewczyk, "Time Dependent Viscous Flow Over a Circular Cylinder," *Physics of Fluids*, Suppl. II, 1969, pp. 79–86.

[2]Gresho, P. M., Lee, R. L., and Sani, R. L., "On the Time-Dependent Solution of the Incompressible Navier-Stokes Equations." *Recent Advances in Numerical Methods in Fluids*, Pineridge Press, Swansea, 1980, pp. 27–80.

[3]Hwang, R. R., Chiang, T. P., and Chiao, M. T., "Time-Dependent Incompressible Viscous Flow Past a Circular Cylinder," *Journal of Chinese Institute of Engineering*, Vol. 9, 1986, pp. 617–631.

[4]Jordan, S. K., and Fromm, J. E., "Oscillatory Drag, Lift, and Torque on a Circular Cylinder in a Uniform Flow," *Physics of Fluids*, Vol. 15, 1972, pp. 371–376.

[5]Lin, C. L., Pepper, D. W., and Lee, S. C., "Numerical Methods for Separated Flow Solutions Around a Circular Cylinder," *AIAA Journal*, Vol. 14, 1976, pp. 900–907.

[6]Patel, V. A., "Karman Vortex Street Behind a Circular Cylinder by the Series Truncation Method," *Journal Computational Physics*, Vol. 28, 1978, pp. 14–42.

[7]Lecointe, Y., and Piquet, J., "On the Use of Several Compact Methods for the Study of Unsteady Incompressible Viscous Flow Around a Circular Cylinder," *Computational Fluids*, Vol. 12, 1984, pp. 255–280.

[8]Smith, S. L., and Brebbia, C. A., "Improved Stability Techniques for the Solution of N-S Equations," *Applied Mathematical Modeling*, Vol. 1, 1977, pp. 227–234.

[9]Jain, P. C., and Goel, B. S., "A Numerical Study of Unsteady Laminar Forced Convection from a Circular Cylinder," *Journal of Heat Transfer*, 1976, pp. 303–307.

[10]McAdam, W. H., *Heat Transmission*, McGraw-Hill, New York, 1954.

[11]Kramers, H. A., "Heat Transfer From Sphere to Flowing Media," *Physics*, Vol. 12, 1946, pp. 61–80.

[12]Van der Hegge Zijnen, B. G., *Applied Science Research*, Vol. A6, 1956, pp. 129.

[13]Tsubouchi, T., and Masuda, A. H., Rept. No. 191, Institute of High Speed Mechanics, Tohoku Univ., Japan, 1966.

[14]Karniadakis, G. E. M., "Numerical Simulation of Forced Convection Heat Transfer from a Cylinder in Crossflow," *International Journal of Heat Mass Transfer*, Vol. 31, No. 1, 1988, pp. 107–118.

[15]Rubin, S. G., and Graves, R. A., "Viscous Flow Solution with a Cubic Spline Approximation, Computers and Fluids," Vol. 3, 1975, pp. 1–36.

[16]Thompson, J. F., Thames, F. C., Mastin, C. W., and Shanks, S. P., "Use of Numerically Generated Body-Fitted Coordinate Systems for Solution of the Navier-Stokes Equations," *Proceeding of the AIAA 2nd Computational Fluid Dynamics Conference*, Hartford, CT, 1975.

Electron Temperature and Electron Density in a Rarefied Air Plasma Jet

M. A. Dudeck,* P. Lasgorceix,† C. Voisin,‡ and S. Cayet§
Centre National de la Recherche Scientifique, Meudon 92190, France

Introduction

AIR jets at low pressure and high temperature are used to simulate some properties of the gas layer surrounding a spacecraft while re-entering the atmospheric zone. Various experimental setups have been developed in order to realize these jets. Hypersonic simulations at low pressure are obtained in wind tunnels[1] working continuously or transient wind tunnels, to measure force, flow, surface temperature, and turbulence. During a re-entry, real gas effects appear between the shock wave and the surface. It concerns especially chemical, ionization, and vibrational nonequilibrium effects. Some of these effects can be studied in air by shock tubes[2–4] or by microwave discharge techniques[5,6] and by arc jets.[7–10] Arc jets can be used to obtain a stationary and large plasma jet arc, but the main difficulty in producing arc jets in a wind tunnel lies in the destruction of electrodes due to the presence of oxygen. A solution may be obtained by injecting oxygen into the nozzle, after the arc.[8,10] This paper presents a generator that produces steady plasma arc jets directly from air for about 1 h at a pressure of 0.08 Torr. Radial profiles of temperatures and densities measured by an electrostatic probe are shown. Electrostatic probe method gives electron density and electron temperature with a good spatial resolution and a characteristic time function of the frequency of the probe potential. Difficulties may appear in the analysis of the probe characteristic, total current collected by the surface probe as a function of probe potential (fluctuations, theory). Electrostatic probes have been used in different types of air plasmas. Single-electrode Langmuir probe measurements have been performed in air at a static pressure of 30 Torr to study the electron attachment by the addition of small quantities of an electrophilic gas.[8] Spherical double probes[6] have been used in air plasma generated by microwaves (900 MHz) in the pressure range 1–10 Torr. The ion density has been measured in air shock tube at initial pressure of 0.075–1.2 Torr by a hollow electrostatic probe at a large negative potential.[5] A thin-wire Langmuir probe[2] has been used in shock tunnel flows to determine the electron density and the electron temperature to deduce the reaction rate coefficient for the reaction $NO^+ + e$. A set of tungsten electrostatic probes has been tested[3] in a hypersonic shock tunnel flow to perform analyses in air. The effects of the probe length, diameter, ratio of probe radius to Debye length, angle of attack, and length-to-diameter ratio are studied. In an arc-heated shock tube at initial pressures 0.1 and 1 Torr, the ion saturation currents have been measured in air with flush electrostatic probes.

Received Oct. 27, 1989; revision received Dec. 31, 1990; accepted for publication Jan. 2, 1991.

*Professor, Laboratoire d'Aérothermique du CNRS, 4ter, Route des Gardes.

†Research Scientist, Laboratoire d'Aérothermique du CNRS, 4ter, Route des Gardes.

‡Research Engineer, Laboratoire d'Aérothermique du CNRS, 4ter, Route des Gardes.

§Graduate Student, Laboratoire d'Aérothermique du CNRS, 4ter, Route des Gardes.